I&EC research
Industrial & Engineering Chemistry Research

Article

pubs.acs.org/IECR

Mechanistic Features of Ultrasound-Assisted Oxidative Desulfurization of Liquid Fuels

Manohar Kumar Bolla,[†] Hanif A. Choudhury,[‡] and Vijayanand S. Moholkar[†,‡,*]

[†]Department of Chemical Engineering and [‡]Center for Energy, Indian Institute of Technology—Guwahati, Guwahati − 781 039, Assam, India

Supporting Information

ABSTRACT: A new technology for the removal of sulfur compounds from liquid fuels is oxidative desulfurization. Although several studies have reported the enhancement effect of ultrasound irradiation on oxidative desulfurization, the exact mechanism underlying this enhancement is not known yet. In this study, we have addressed this issue with dual approach of coupling experiments with mathematical model for cavitation. Results of this study have given interesting revelation of interaction between mechanism of ultrasound, cavitation, and oxidation system. Isolation of cavitation phenomenon helps to increase the extent of oxidation. This effect is attributed to formation of hydrogen and carbon monoxide during transient collapse of cavitation bubbles due to thermal dissociation of hexane vapor entrapped in the bubble, which hamper the action of O species generated from the oxidation system. Transient cavitation itself does not give rise to radical formation, because of rather low temperature peaks reached during collapse. Therefore, cavitation does not enhance the oxidation process, but in fact, has an adverse effect on it. Current study has established that the beneficial effect of ultrasound on oxidative desulfurization system is merely of a physical nature (i.e., emulsification due to intense micromixing), with no involvement of a sonochemical effect.

1. INTRODUCTION

Crude oil contains numerous sulfur compounds, mainly in the form of aromatic hydrocarbons such as sulfides, thiols, thiophenes, benzothiophene, dibenzothiophene, and their substituted derivatives. During the distillation and refining of crude oil, these compounds end up in the gasoline and diesel fractions. Combustion of these compounds in vehicle engines results in the generation of SO_2 and the emission of particulate matter. Growing concerns over air pollution created by these emissions have led to stringent restrictions on the sulfur content of the liquid fuels. To meet these specifications, the quest is on for technologies for deep desulfurization that could give ultralow sulfur diesel (ULSD). A conventional technique for the desulfurization of diesel and petrol practiced by petroleum industry is hydrotreating or catalytic hydrodesulfurization, in which the sulfur in the hydrocarbons is removed as H_2S. However, this technique has poor economics and requires harsh conditions of temperatures (>300 °C) and pressures (>30 bar). Moreover, there are other limitations such as negligible removal of substituted benzothiophenes and dibenzothiophenes, because of their low reactivity.

Another new technology that has emerged for the deep desulfurization of diesel and petrol is oxidative desulfurization, in which the sulfur-containing compounds are initially oxidized to respective sulfones, and later are extracted using a suitable solvent such as dimethylsulfoxide (DMSO), dimethylformamide (DMF), and acetonitrile. The technology of oxidative desulfurization has several merits over the conventional hydrotreatment, including (i) it does not require the use of expensive hydrogen, (ii) the treatment conditions (i.e., temperature and pressure) are almost ambient, and (iii) effective oxidation (and, hence, removal by liquid extraction) of the substituted sulfur aromatics (which are recalcitrant to hydrotreating) is observed. The oxidants commonly employed are peroxy organic acids, hydroperoxides, nitrogen oxides, peroxy salts, and ozone. These oxidants donate oxygen atoms to the sulfur in the aromatic hydrocarbons. Being simple and effective, this technique has high potential for implementation on a large scale. More recently, oxidative desulfurization has been coupled with ultrasound irradiation.[1−6] This new technique is reported to enhance the kinetics, as well as the yield, of the oxidative desulfurization process. Most of the studies published earlier have emphasized the results of ultrasonic oxidative desulfurization, and few attempts have been dedicated to exploring the exact mechanism underlying the beneficial actions of ultrasound on the reaction system, which is essentially a biphasic liquid−liquid heterogeneous system. In this paper, we have addressed the matter of discerning the mechanism of ultrasound-enhanced oxidative desulfurization. Our approach is to couple experimental results (with model sulfur compounds and oxidants) with simulations of cavitation bubble dynamics. Before proceeding to the main components of the study, we outline briefly the physical and chemical effects of ultrasound and cavitation on a process. The principal chemical effect of cavitation bubbles is the generation of radicals through the dissociation of vapor molecules entrapped in the bubble under the extreme conditions of temperature and pressure (~5000 K and ~500 bar) generated in the bubble at transient collapse. The physical effect of ultrasound is creation convection in the medium through small amplitude oscillatory

Received: March 26, 2012
Revised: June 17, 2012
Accepted: June 25, 2012
Published: June 25, 2012

dx.doi.org/10.1021/ie300807a | *Ind. Eng. Chem. Res.* 2012, 51, 9705−9712

motion of fluid elements around a mean position, known as microstreaming. Cavitation also generates convection in the medium, however; there are several mechanism associated with the convection generated by cavitation such as microturbulence (which is oscillatory liquid velocity generated by bubble), shock waves and high-speed microjets (generated due to asymmetric collapse of bubble in the vicinity of a phase boundary with magnitude of 120−150 m/s). For greater on these mechanisms, we refer the reader to our earlier paper.[7] For a liquid−liquid heterogeneous reaction system such as oxidative desulfurization of petrol and diesel, both physical and chemical effects of cavitation influence kinetics and yield of the reaction. Intense microturbulence created by the cavitation bubbles disrupts the liquid/liquid interface and creates very fine emulsion between the phases. This greatly enhances the interfacial area and obviates need for additional agents for mass-transfer enhancement, such as phase-transfer catalysts.

2. MATERIALS AND METHODS

2.1. Materials. Following chemicals were used in the experiments: benzothiophene, thiophene, 3-methyl thiophene, 30% hydrogen peroxide, iron(II) sulfate heptahydrate (for Fenton's reagent), *n*-hexane and acetic acid (or peracetic acid). All chemicals were procured from Merck (analytical grade) and were used as received without any pretreatment.

2.2. Methods. The major parameter varied in the experiments of the present study was system pressure. We conducted our experiments under two static pressures, viz. atmospheric (1 bar) and elevated to 1.5 bar gauge (or an absolute pressure of 2.5 bar). The rationale underlying this technique will be discussed in the next section. An ultrasound bath (Transonic T-460 type, Germany, 2 L), which operates at a frequency of 35 kHz and power of 35 W was used for sonication of the medium. The power rating of the ultrasound bath (35 W) corresponds to theoretical (or maximum) ultrasound intensity. The actual ultrasound power delivered to the medium was determined using a calorimetric technique.[8] Per calorimetric measurements, for a theoretical intensity of 35 W, the ultrasound bath produced an acoustic wave of 1.5 atm pressure amplitude. However, the ultrasound wave undergoes attenuation as it passes through the medium and hence the actual pressure amplitude sensed by the cavitation bubble is <1.5 atm.

2.3. Calibration Experiments. Prior to main experiments, calibration charts were prepared using known quantities of three model sulfur compounds, viz, benzothiophene, thiophene, and 3-methyl thiophene dissolved in *n*-hexane, which was the model petrol. The charts showed an excellent linearity for thiophene (concentration range 0−1000 mg/dm^3), benzothiophene (concentration range 0−1000 mg/dm^3), and 3-methyl thiophene (concentration range 0−1000 mg/dm^3). The analysis was performed using HPLC with a Hibar-Purospher-STAR RP-18 column (Merck) and UV detector at λ = 271 nm. The mobile phase was composed of acetonitrile and water in 4:1 volumetric ratio, at a flow rate of 0.7 cm^3/s.

2.4. Oxidation Experiments. Three model oxidants used in this study were (1) $CH_3COOH + H_2O_2$ (peracetic acid), (2) $CH_3COOH + H_2O + H_2O_2$ (diluted peracetic acid), (3) $CH_3COOH + H_2O_2 + Fe^{2+}$ (peracetic acid + Fenton's reagent). Oxidation of the three model sulfur compounds used in this study (viz, thiophene, 3-methyl thiophene, and benzothiophene) is represented by the following reactions:

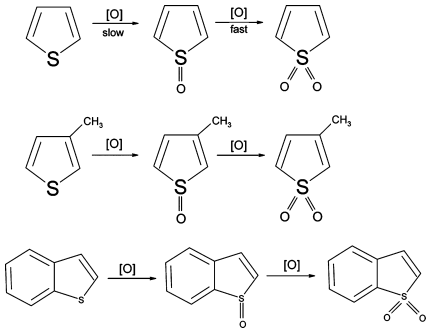

A schematic diagram of the experimental setup is given in the Supporting Information (Figure A.1). In a typical experiment, initially, a solution of a particular model sulfur compound in *n*-hexane (25 mL) was prepared in the desired concentration (either 100, 300, or 500 ppm) in a conical flask with a volume of of 100 mL. Twenty-five milliliters (25 mL) of the desired oxidant was added to this solution, which resulted in a heterogeneous liquid mixture with a volumetric ratio of 1:1. The initial temperature of solution was 298 K (25 °C). In each experiment, two-thirds of the bath was filled with water. The conical flask was placed at the center of the ultrasound bath for the entire experiment. The intensity of the ultrasound field in the bath shows significant spatial variation. Therefore, to avoid the change of intensity of the ultrasound field to which the flask is exposed, the position of the flask in the bath was carefully maintained constant during the entire experiment with the help of a burette stand and clamp. A simple arrangement was used to raise the static pressure in the conical flask. The mouth of the flask was sealed using a rubber cork with a central tube pierced in it. The outer end of the tube was connected to a nitrogen gas cylinder with a double-stage regulator. The water in the bath was replaced every 10 min to maintain the constant temperature of reaction mixture during sonication. The average temperature of the bath, and the reaction mixture in conical flask, varied by <2 °C due to this procedure. In order to monitor the kinetics of degradation, samples of the reaction solution (5 mL) were withdrawn every 15 min for HPLC analysis.

3. BUBBLE DYNAMICS MODEL

Modeling of cavitation bubble dynamics is an active area of research for the past three decades. A review of previous studies in this area has been presented by Krishnan et al.[9] We have used the diffusion-limited ordinary differential equation (ODE) model (using boundary-layer approximation) proposed by Toegel et al.[10] for our analysis, which is based on the comprehensive partial differential equation (PDE) model of Storey and Szeri,[11] who showed that vapor entrapment in the cavitation bubble, leading to the formation of radicals, is essentially a diffusion-limited process. This model has been extensively described in our previous papers.[8,9] For the convenience of the reader, here, we reproduce only the main components of the model and relevant data/boundary conditions.

The essential equations and thermodynamic data of this model have been summarized in Tables 1 and 2.[10,12−16] The main components of the model are (1) the Keller−Miksis equation for the radial motion of the bubble, (2) an equation for the diffusive flux of water vapor and heat conduction through bubble wall, and (3) the overall energy balance. The transport parameters for the heat and mass transfer (thermal conductivity and diffusion coefficient) are determined using Chapman−Enskog theory, using Lennard-Jones 12−6 potential

dx.doi.org/10.1021/ie300807a | Ind. Eng. Chem. Res. 2012, 51, 9705−9712

Table 1. Model for the Radial Motion of Cavitation Bubble[a]

model component	equation	initial value
1. Radial motion of the cavitation bubble	$\left(1-\frac{dR/dt}{c}\right)R\frac{d^2R}{dt^2}+\frac{3}{2}\left(1-\frac{dR/dt}{3c}\right)\left(\frac{dR}{dt}\right)^2 = \frac{1}{\rho_L}\left(1+\frac{dR/dt}{c}\right)(P_i-P_t)+\frac{R}{\rho_L c}\frac{dP_i}{dt}-4\nu\frac{dR/dt}{R}-\frac{2\sigma}{\rho_L R}$ Internal pressure in the bubble: $P_i=\frac{N_{tot}(t)kT}{[4\pi(R^3(t)-h^3)/3]}$ Pressure in bulk liquid medium: $P_t=P_0-P_A\sin(2\pi ft)$	At $t=0$, $R=R_0$ $dR/dt=0$
2. Diffusive flux of *n*-hexane molecules	$\frac{dN_H}{dt}=4\pi R^2 D_H\left.\frac{\partial C_H}{\partial r}\right\|_{r=R}\approx 4\pi R^2 D_H\left(\frac{C_{H,R}-C_H}{l_{diff}}\right)$ Instantaneous diffusive penetration depth: $l_{diff}=\min\left(\sqrt{\frac{RD_H}{\lvert dR/dt\rvert}},\frac{R}{\pi}\right)$	At $t=0$, $N_H=0$
3. Heat conduction across bubble wall	$\frac{dQ}{dt}=4\pi R^2\lambda\left.\frac{\partial T}{\partial r}\right\|_{r=R}\approx 4\pi R^2\lambda\left(\frac{T_0-T}{l_{th}}\right)$ Thermal diffusion length: $l_{th}=\min\left(\sqrt{\frac{R\kappa}{\lvert dR/dt\rvert}},\frac{R}{\pi}\right)$	At $t=0$, $Q=0$
4. Overall energy balance	$C_{V,mix}\frac{dT}{dt}=\frac{dQ}{dt}-P_i\frac{dV}{dt}+(h_H-U_H)\frac{dN_H}{dt}$ Mixture heat capacity: $C_{V,mix}=\sum C_{V,i}N_i$ ($i=N_2/O_2/n$-hexane) Molecular properties of *n*-hexane: Enthalpy: $h_H=4kT_0$ Internal energy: $U_H=N_HkT\left[3+\sum_{i=1}^{3}\frac{\theta_i/T}{\exp(\theta_i/T)-1}\right]$ Heat capacity of various species ($i=N_2/O_2/n$-hexane): $C_{V,i}=N_ik\left\{\frac{f_i}{2}+\sum\frac{(\theta_i/T)^2\exp(\theta_i/T)}{[\exp(\theta_i/T)-1]^2}\right\}$	At $t=0$, $T=T_0$
Convection generated due to cavitation	$V_{turb}(r,t)=\frac{R^2}{r^2}\left(\frac{dR}{dt}\right)$ Shock waves (or acoustic waves): $P_{AW}(r,t)=\frac{\rho_L}{4\pi r}\frac{d^2V_b}{dt^2}=\rho_L\frac{R}{r}\left[2\left(\frac{dR}{dt}\right)^2+R\frac{d^2R}{dt^2}\right]$	

[a]Notations: R, radius of the bubble; dR/dt, bubble wall velocity; c, velocity of sound in bulk liquid medium; ρ_L, density of the liquid; ν, kinematic viscosity of liquid; σ, surface tension of liquid; λ, thermal conductivity of bubble contents; κ, thermal diffusivity of bubble contents; θ, characteristic vibrational temperature(s) of the species; N_H, number of hexane molecules in the bubble; N_{N_2}, number of nitrogen molecules in the bubble; N_{O_2}, number of oxygen molecules in the bubble; t, time, D_H, diffusion coefficient of *n*-hexane vapor; C_H, concentration of *n*-hexane molecules in the bubble; $C_{H,R}$, concentration of *n*-hexane molecules at the bubble wall or gas/liquid interface; Q, heat conducted across bubble wall; T, temperature of the bubble contents; T_0, ambient (or bulk liquid medium) temperature; k, Boltzmann constant; h_H, molecular enthalpy of *n*-hexane; U_H, internal energy of *n*-hexane molecules; f_i, translational and rotational degrees of freedom; $C_{V,i}$, heat capacity at constant volume for species i; N_{tot}, total number of molecules (gas + vapor) in the bubble; h, van der Waal's hard core radius; P_0, ambient (bulk) pressure in liquid; P_A, pressure amplitude of ultrasound wave; f, frequency of ultrasound wave; V_b, volume of the bubble; r, distance from bubble center at which microturbulence velocity is estimated (representative value taken as 1 mm); V_{turb}, velocity of microturbulence; and P_{AW}, pressure amplitude of the acoustic (or shock waves) emitted by the bubble.

at the bulk temperature of the liquid medium. Thermal and diffusive penetration depths are estimated using dimensional analysis. Diffusion of gas across the bubble interface is ignored in the present model, because the time scale for the diffusion of gases is much higher than the time scale for the radial motion of bubble. The set of four ODEs described in Table 1 was solved simultaneously using the Runge−Kutta adaptive step size method.[17] We have considered an air bubble for simulations as the cavitation in solvent (i.e., *n*-hexane) occurred, due to in situ nuclei, comprised of air. The condition for bubble collapse is taken as the first compression after an initial expansion. Various parameters used in the simulation of bubble dynamics equation and their numerical values are as follows: ultrasound frequency (f) = 20 and 35 kHz for sonicator probe and ultrasound bath, respectively; ultrasound pressure amplitude (P_A) = 1.3 bar; equilibrium bubble radius (R_0) = 5 and 10 μm; the vapor pressure of the liquid medium (*n*-hexane) was calculated using an Antoine-type correlation. Various physical properties of *n*-hexane are as follows: density (ρ_L) = 658 kg/m^3, kinematic viscosity (ν) = 5×10^{-7} Pa s, surface tension (σ) = 0.0179 N/m, and velocity of sound (c) = 1203 m/s.

dx.doi.org/10.1021/ie300807a | Ind. Eng. Chem. Res. 2012, 51, 9705−9712

Table 2. Thermodynamic Properties of Various Species[a,b]

species	degrees of freedom (translational + rotational), f_i	Lennard-Jones Force Constants σ ($\times 10^{-10}$ m)	Lennard-Jones Force Constants ε/k (K)	characteristic vibrational temperature(s), θ (K)
N_2	5	3.68	92	3350
O_2	5	3.43	113	2273
n-hexane	6	5.75	386.4	1035.71, 1932.31, 1987.43, 2104.17, 4193.26

[a]Data taken from refs 21−25. [b]See Table 1 for an explanation of the parameters used in this table.

3.1. Estimation of Sonochemical Effect (Radical Generation by Cavitation Bubbles). Using the numerical solution of a bubble dynamics model, one can estimate the composition of the bubble contents at the collapse. While calculating the composition of the bubble at the time of collapse, we assume that thermodynamic equilibrium is attained.[9] The equilibrium mole fraction of the various species in the bubble under the conditions of temperature and pressure at the first compression of the bubble can be calculated using the Gibbs free-energy minimization technique.[18]

4. RESULTS AND DISCUSSION

As noted in Section 3, we have conducted our experiments under atmospheric and elevated static pressure. Before proceeding to the main results and discussion section, we would like to discuss the rational underlying the application of elevated pressure. Irradiation of a liquid medium with ultrasound (which is essentially a longitudinal wave) leads to the occurrence of two phenomena: (1) high velocity oscillation of fluid elements around their mean position, giving alternate compression and rarefaction cycles, and (2) the phenomenon of cavitation, which is nucleation growth and transient collapse of the gas/vapor bubbles driven by bulk pressure variation due to the ultrasound wave. The first phenomenon creates intense micromixing in the medium, while the second phenomenon, which is of secondary nature, can give rise to two effects: (1) the physical effect of micromixing or microturbulence due to liquid set into motion by volume oscillations of the bubble, and (2) generation of radical species due to dissociation of the solvent vapor entrapped in the bubble at the moment of transient collapse. The intensity of the collapse of the bubble depends on its expansion during the rarefaction cycle of ultrasound where the bulk pressure in the system falls below atmospheric pressure. The greater the fall of the system pressure below ambient, the larger the expansion of the bubble, and the more intense the ensuring collapse.

To distinguish between the physical and chemical effects, the expansion of the bubble must be suppressed. This could be achieved by raising the ambient or static pressure in the system above the pressure amplitude of the ultrasound wave. As noted in Section 3, the amplitude of the ultrasound generated by ultrasound bath used in this study was 1.5 atm. Therefore, raising the static pressure to 1.5 atm (gauge) or a total absolute pressure of 2.5 atm, could suppress all transient cavitation in the system and, thus, help distinguish the influence of micromixing due to ultrasound itself. With this preamble, we first present the experimental results followed by the simulations results. Next, we correlate these results to deduce the exact mechanism of the ultrasound-assisted oxidative desulfurization.

4.1. Experimental Results. The trends in the oxidation of three model sulfur compounds at atmospheric and elevated static pressure are shown in Figures 1, 2, and 3 for the oxidants

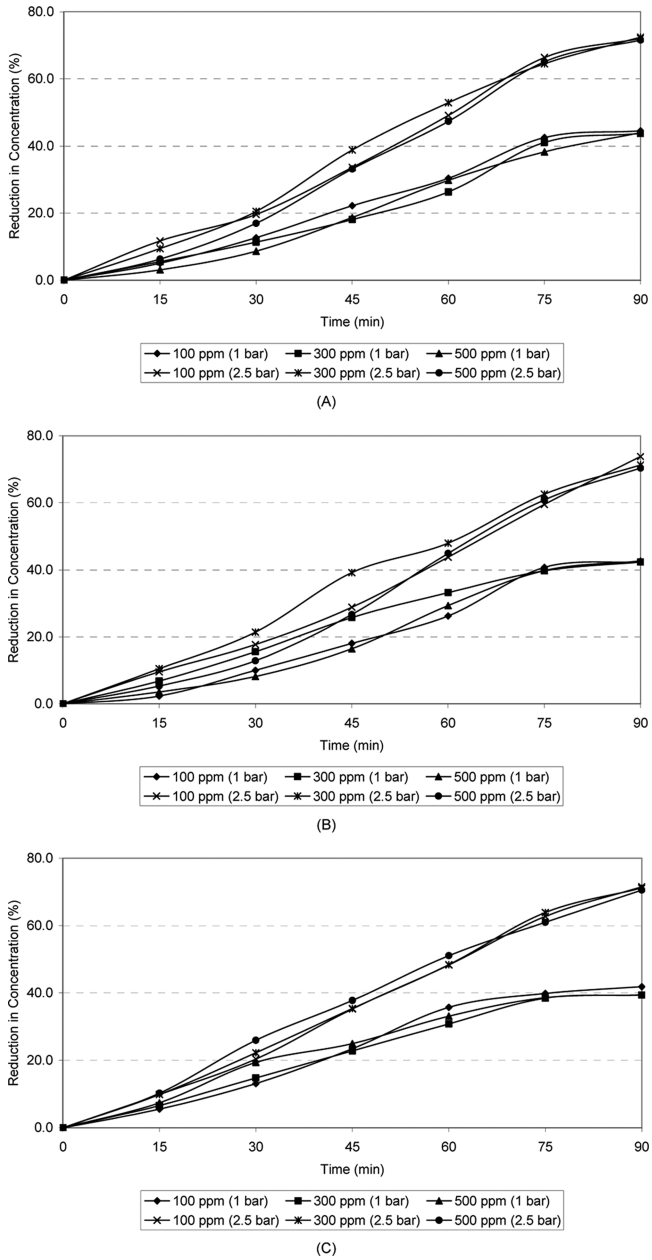

Figure 1. Trends in the oxidative desulfurization (represented as reduction in the concentration of the model sulfur compound) with oxidant peracetic acid ($CH_3COOH + H_2O_2$): (A) oxidation of benzothiophene, (B) oxidation of 3-methyl thiophene, and (C) oxidation of thiophene.

peracetic acid, diluted peracetic acid and Fenton's reagent supplemented peracetic acid, respectively. In order to quantify the rate of oxidation, a first-order kinetics model has been fitted to the reaction data. The entire summary of the results of oxidation experiments is presented in Table 3. Also listed in these tables are the first-order kinetic constants for the oxidation reactions of different compounds. An Excel file giving

dx.doi.org/10.1021/ie300807a | Ind. Eng. Chem. Res. 2012, 51, 9705−9712

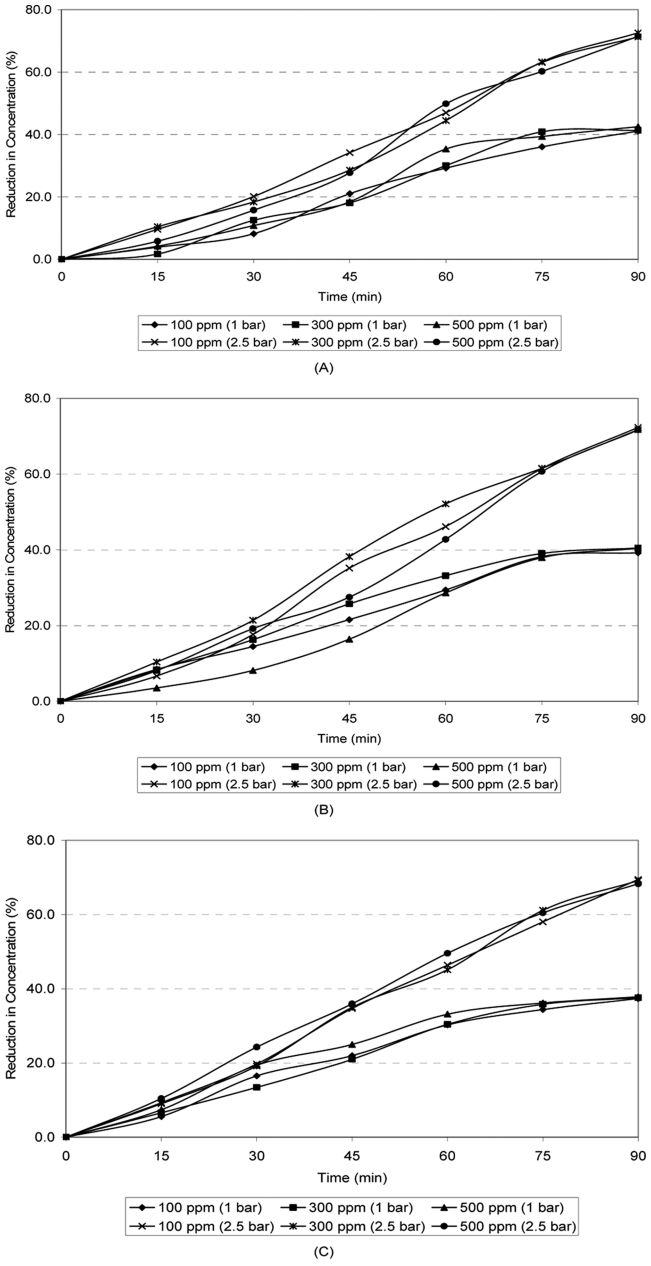

Figure 2. Trends in the oxidative desulfurization (represented as reduction in the concentration of the model sulfur compound) with oxidant diluted peracetic acid ($CH_3COOH + H_2O_2 + H_2O$): (A) oxidation of benzothiophene, (B) oxidation of 3-methyl thiophene, and (C) oxidation of thiophene.

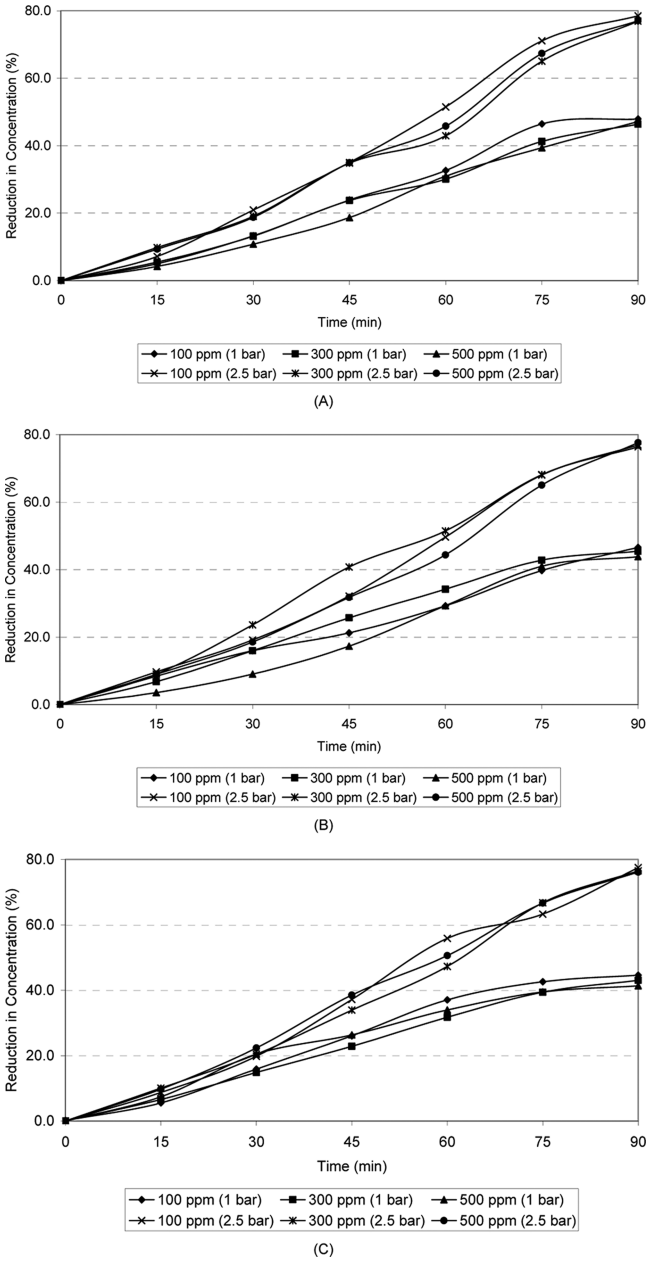

Figure 3. Trends in the oxidative desulfurization (represented as reduction in the concentration of the model sulfur compound) with oxidant peracetic acid supplemented with Fenton's reagent ($CH_3COOH + H_2O_2 + Fe^{2+}$): (A) oxidation of benzothiophene, (B) oxidation of 3-methyl thiophene, and (C) oxidation of thiophene.

greater details of the reaction data for all experiments has been provided as Supporting Information. From the results presented in Figures 1−3 and Table 3, we can identify the following trends in the kinetics of oxidation of model sulfur compounds with different oxidants.

4.1.1. Oxidation System of Peracetic Acid. The extent of oxidation in 90 min of sonication with peracetic acid for atmospheric pressure has the following order: benzothiophene > 3-methyl thiophene > thiophene. For any particular compound, the percentage conversion remains the same, irrespective of the initial concentration. It must be noted, however, that the absolute amount of sulfur compound oxidized increases with initial concentration, which would essentially mean that, in the oxidation mixture used in present experiments, sulfur compounds were the limiting reactant. The kinetic constants observed for these three initial concentrations are also almost the same. A significant increase (~50% or higher) in the kinetics of oxidation as well as extent of oxidation achieved in 90 min of sonication is observed with increases in the static pressure of the reaction mixture.

4.1.2. Oxidation System of Diluted Peracetic Acid. This system gives trends similar to those seen for the peracetic acid; however, the exact of oxidation is reduced marginally for all three model compounds and both sonication systems. The absolute degradation increases with percentage degradation remaining the same for all three compounds shown; that it, is a kinetically limited system with sulfur compound as a limiting reactant. Comparing among the three model compounds,

dx.doi.org/10.1021/ie300807a | Ind. Eng. Chem. Res. 2012, 51, 9705−9712

Table 3. Summary of Experimental Results[a]

			Oxidation System					
			Peracetic Acid $CH_3COOH + H_2O_2$		Diluted Peracetic Acid $CH_3COOH + H_2O_2 + H_2O$		Peracetic Acid + Fenton $CH_3COOH + H_2O_2 + Fe^{2+}$	
sulfur compound	0	C_0 (ppm)	k_1 (min^{-1})	η (%)	k_1 (min^{-1})	η (%)	k_1 (min^{-1})	η (%)
benzothiophene	atmospheric	100	6.2916×10^{-3}	44.5	5.5113×10^{-3}	41.1	6.9163×10^{-3}	47.9
		300	5.7887×10^{-3}	43.7	5.7893×10^{-3}	41.3	6.4055×10^{-3}	46.4
		500	5.7249×10^{-3}	43.9	6.0284×10^{-3}	42.5	6.1097×10^{-3}	47.1
	2.5 bar	100	11.618×10^{-3}	72.0	11.1947×10^{-3}	71.2	12.6085×10^{-3}	79.4
		300	12.068×10^{-3}	72.4	10.7574×10^{-3}	72.5	11.4572×10^{-3}	77.9
		500	11.081×10^{-3}	71.5	10.542×10^{-3}	71.4	11.799×10^{-3}	77.0
3-methyl thiophene	atmospheric	100	5.6055×10^{-3}	42.4	5.7771×10^{-3}	39.2	6.3232×10^{-3}	46.6
		300	6.3963×10^{-3}	42.3	6.2915×10^{-3}	40.5	6.8257×10^{-3}	45.5
		500	5.6129×10^{-3}	42.6	5.361×10^{-3}	40.4	5.8073×10^{-3}	43.9
	2.5 bar	100	10.5077×10^{-3}	73.8	10.9658×10^{-3}	72.3	11.9195×10^{-3}	76.3
		300	11.6049×10^{-3}	71.3	11.7838×10^{-3}	71.7	12.852×10^{-3}	76.9
		500	10.0126×10^{-3}	70.3	10.3323×10^{-3}	71.6	11.3763×10^{-3}	77.6
thiophene	atmospheric	100	6.3179×10^{-3}	41.9	5.5348×10^{-3}	37.4	6.8918×10^{-3}	44.6
		300	5.9007×10^{-3}	39.4	5.5235×10^{-3}	37.6	6.2127×10^{-3}	43.0
		500	6.2525×10^{-3}	39.5	6.019×10^{-3}	37.8	6.5446×10^{-3}	41.4
	2.5 bar	100	11.355×10^{-3}	71.5	10.6769×10^{-3}	69.4	12.4013×10^{-3}	77.5
		300	11.517×10^{-3}	71.1	10.7808×10^{-3}	69.4	11.8577×10^{-3}	76.5
		500	11.7877×10^{-3}	70.5	11.2877×10^{-3}	68.5	12.4248×10^{-3}	76.1

[a]Legend: k_1, first-order kinetic constant; C_0, initial concentration of the sulfur compound in *n*-hexane; and η, percentage oxidation of sulfur compound calculated as [100 × (initial concn. − final concn.)/initial concn.].

we see the exact same trend as that seen for peracetic acid. Similarly, the kinetics of oxidation—and, hence, the extent of oxidation in 90 min of sonication—also increases as the static pressure of the reaction medium increases.

4.1.3. Oxidation System of Peracetic Acid + Fenton's Reagent. This system gives a higher oxidation than percacetic acid and diluted peracetic acid for all three compounds, but the enhancement over the peracetic acid is rather marginal. In this system, Fenton's reagent ($Fe^{2+} + H_2O_2$) is expected to generate additional oxidants through the reactions

$$Fe^{2+} + H_2O_2 \rightarrow Fe^{3+} + OH^- + {}^{\bullet}OH \quad (1)$$

$$Fe^{3+} + H_2O \rightarrow H^+ + FeOOH^{2+} \quad (2)$$

$$FeOOH^{2+} \rightarrow HO_2^{\bullet} + Fe^{2+} \quad (3)$$

However, this generation has not seen to give a marked enhancement over the peracetic acid system. It should be noted that the principal radical generated in the Fenton's reagent system is ${}^{\bullet}OH$ (and not ${}^{\bullet}O$), and, thus, it may not be much useful in the oxidation chemistry. Nevertheless, the ${}^{\bullet}OH$ radical can give conservation of radicals in the system, which would facilitate generation as well as effective utilization of the $O^{\bullet}$ radicals that result in greater oxidation, as explained in greater detail in the next section.[19] Similar to the peracetic acid system, the initial concentration of the model compound does not affect the percentage oxidation. Nevertheless, absolute degradation increases with initial concentration, making it a kinetically limited system with model compound as a limiting reagent. Finally, in the case of this oxidation system as well, we observe a marked increase in the kinetic constant of oxidation, as well as the extent of oxidation in 90 min of sonication.

4.2. Simulation Results. The summary of the simulation results is given in Table 4, which lists (i) the temperature and pressure peaks reached during bubble collapse (i.e., the first compression of the bubble after an initial expansion); (ii) the number of nitrogen, oxygen, and hexane molecules present in the bubble; and (iii) the equilibrium composition of the species resulting from thermal dissociation of the hexane molecules at the collapse conditions. Figures A.2−A.5 in the Supporting Information give pictorial depictions of the simulation results for the radial motion of 5- and 10-μm air bubbles for atmospheric static pressure in a reaction system. We can identify following distinct trends in the simulation results:

(1) Both 5- and 10-μm bubbles undergo an intense collapse at 1 bar ambient pressure to generate a broad spectrum of various radical and molecular species. The dominant molecular species are H_2, CO, and CH_4. At elevated pressure, however, the radial motion of both bubbles is rather a stable oscillatory type, and the temperature in the bubble remains close to ambient.

(2) Comparing bubbles between 5 and 10 μm in size, we find that the temperature and pressure peaks reached in the collapse of 5-μm bubble are much higher than the 10-μm bubble. However, the entrapment of vapor molecules is relatively small.

(3) Looking at the spectrum of the species resulting from the thermal dissociation of entrapped vapor molecules in the transient collapse of both 5- and 10-μm bubbles at atmospheric pressure, we find practically no radical species generation (as typically seen in the case of water as the medium). Predominantly small hydrocarbon molecules such as CH_4, CO_2, C_2H_4, and C_2H_6 are generated with H_2 and CO. The radial bubble motion at elevated pressure is of an oscillatory nature, and the temperature and pressure in the bubble do not show any significant rise. In this case, the principal products of thermal dissociation of hexane are CH_4 and H_2O, with small quantities

dx.doi.org/10.1021/ie300807a | Ind. Eng. Chem. Res. 2012, 51, 9705−9712

Table 4. Summary of Simulations Results

Conditions at the First Collapse of the Bubble at Various Parameters for Simulation (Temperature: 298 K)				
parameter[a]	R_0 = 5 μm, P_0 = 1 atm	R_0 = 10 μm, P_0 = 1 atm	R_0 = 5 μm, P_0 = 2.5 atm	R_0 = 10 μm, P_0 = 2.5 atm
T_{max} (K)	1151	1114	339	366
P_{max} (atm)	446	375	4	5
N_{N_2}	1.09×10^{10}	8.42×10^{10}	1.09×10^{10}	8.42×10^{10}
N_{O_2}	2.89×10^{9}	2.24×10^{10}	2.89×10^{9}	2.24×10^{10}
N_{HT}	6.05×10^{10}	2.06×10^{11}	1.97×10^{9}	2.04×10^{10}
V_{turb} (mm/s)	4.5	33	4.51×10^{-2}	0.36
P_{AW} (kPa)	180	640	0.13	0.81
Equilibrium Composition of Various Species in the Bubble at the Transient Collapse (Mole Fraction)				
species	R_0 = 5 μm, P_0 = 1 atm	R_0 = 10 μm, P_0 = 1 atm	R_0 = 5 μm, P_0 = 2.5 atm	R_0 = 10 μm, P_0 = 2.5 atm
N_2	4.72×10^{-2}	1.01×10^{-1}	7.34×10^{-1}	5.69×10^{-1}
O_2	0	0	0	0
CO	3.98×10^{-3}	7.04×10^{-3}	0	0
H_2	2.54×10^{-1}	2.27×10^{-1}	4.93×10^{-5}	1.44×10^{-4}
CO_2	2.85×10^{-4}	1.34×10^{-3}	3.13×10^{-4}	2.39×10^{-3}
CH_4	6.70×10^{-1}	6.15×10^{-1}	2.03×10^{-1}	2.66×10^{-1}
C_2H_4	3.16×10^{-5}	1.86×10^{-5}	0	0
C_2H_6	1.79×10^{-4}	1.49×10^{-4}	0	0
NH_3	3.06×10^{-3}	3.84×10^{-3}	9.61×10^{-5}	1.40×10^{-4}
H_2O	2.13×10^{-2}	4.52×10^{-2}	6.21×10^{-2}	1.62×10^{-1}
HCN	4.58×10^{-6}	3.98×10^{-6}	0	0

[a]Notation: T_{max}, temperature peak reached in the bubble at transient collapse; P_{max}, pressure peak reached in the bubble at transient collapse; N_{N_2}, number of nitrogen molecules in the bubble; N_{O_2}, number of oxygen molecules in the bubble; N_{HT}, number of hexane molecules entrapped in the bubble; V_{turb}, velocity of microturbulence; and P_{AW}, pressure amplitude of the acoustic (or shock waves) emitted by the bubble.

of hydrogen and CO_2. No CO formation is observed at elevated pressure.

(4) The convection generated in the reaction mixture during sonication is a combined effect of ultrasound waves and cavitation bubbles. As noted earlier, cavitation bubbles generate convection in the medium through microturbulence and acoustic waves. Table 4 gives values of these two quantities (represented by V_{turb} and P_{AW}) for the bubbles of 5 and 10 μm in size. As the static pressure in the medium increases, the intensity of the microturbulence and the acoustic waves generated by the bubbles reduces drastically. The magnitude of microstreaming generated by ultrasound waves is given as[20]

$$u = \frac{P_A}{\rho_L c}$$

where c is the sonic velocity in the medium (1203 m/s for *n*-hexane) and ρ_L is the density of the medium (658 kg/m^3 for *n*-hexane). Thus, for an acoustic pressure amplitude of 1.5 bar (as in the case of the ultrasound bath used in the present study), the microstreaming velocity is 0.19 m/s. Comparing this value against V_{turb} for both atmospheric and elevated static pressure (for both 5- and 10-μm bubbles), it could be deduced that the contribution of ultrasound to the overall convection is much higher than the cavitation bubbles. However, note that the intensity of microstreaming, i.e., oscillatory liquid velocity generated by ultrasound wave, in the reaction system is not influenced much by the elevated pressure, as the liquid-phase properties such as density, viscosity, and surface tension are a very weak function of the static pressure of the medium.

4.3. Analysis. Analysis of the experimental results reveals interesting features of ultrasound-assisted oxidative desulfurization, which are summarized below:

(1) Oxidation is found to follow first-order kinetics for all three sulfur compounds. No generation of any radical species during transient collapse of cavitation bubbles of both sizes indicates that the influence of ultrasound and cavitation on the reaction system is of merely physical nature. Intense turbulence generated by ultrasound and cavitation generates a fine emulsion of *n*-hexane (organic medium) with the oxidation system (aqueous medium), due to which interfacial area increases drastically resulting in rise in the kinetics of oxidation.

(2) Higher degradation is observed in the case of peracetic acid with Fenton's reagent, which is essentially due to additional generation of the oxidant species by reaction of $^{\bullet}OH$ radicals generated from Fenton's reactions with the dissolved oxygen in the system through the reaction

$$^{\bullet}OH + O_2 \rightleftarrows HO_2^{\bullet} + O^{\bullet}$$

The dissolved oxygen content of the medium is relatively independent of the static pressure of the medium; hence, the above effect is present in experiments at both atmospheric pressure and raised static pressure.

(3) The most interesting experimental result, which is consistent for all three oxidation systems employed, is the increase in oxidation of all three sulfur compounds with the application of higher pressure to the reaction system. A plausible reason for this effect could be given by analysis results and simulation. As noted in the previous section, the predominant species generated from the thermal dissociation of *n*-hexane during the transient collapse of cavitation bubbles in the reaction system at atmospheric pressure are hydrogen and carbon monoxide. These species can competitively consume the $O^{\bullet}$ species generated by the oxidation system. Thus, the utilization of the $O^{\bullet}$ species toward the oxidation of sulfur compounds is limited, which reduces the extent of oxidation.

(4) With the application of elevated pressure, the transient cavitation in the system is eliminated. The cavitation bubbles undergo stable oscillatory motion, with very small generation of H_2 and practically no generation of CO. The intensity of microturbulence as well as shock waves generated by bubbles also decreases as the static pressure increases. However, as stated in section 4.3, the convection generated in the reaction mixture during sonication is mostly contributed by ultrasound waves, which is not affected by an increase in static pressure. Hence, the extent of emulsification and interfacial area for reaction is not influenced by the rise in static pressure. The net consequence of these effects is that the $O^{\bullet}$ species generated by the oxidation system are effectively utilized for the oxidation of the sulfur compounds, which results in an increase in oxidation kinetics and yield.

dx.doi.org/10.1021/ie300807a | Ind. Eng. Chem. Res. 2012, 51, 9705−9712

5. CONCLUSIONS

In this study, we have attempted to identify the mechanistic features of the beneficial action of ultrasound irradiation on an oxidative desulfurization reaction system, which essentially is a liquid−liquid heterogeneous system. Concurrent analysis of experimental and simulations results reveals that the beneficial action of ultrasound on oxidative desulfurization is merely by the physical effect of intense microconvection generated in the system, which causes a fine emulsification of fuel and oxidant, and generates high interfacial area between fuel and oxidant. An anomaly of the oxidative desulfurization system with conventional sonochemical systems is that occurrence of transient cavitation in the medium is revealed to affect the process adversely. This is a consequence of the generation of chemical species such as hydrogen and carbon monoxide that competitively consume the oxidant species, thus hindering the oxidation of sulfur compounds. The elimination of transient cavitation by a simple technique of raising static pressure of the system is found to give a significant boost to the oxidation process, because of the efficient utilization of oxidizing species for the oxidation for sulfur compounds.

■ ASSOCIATED CONTENT

Ⓢ Supporting Information

The following supporting information has been provided with this paper: (1) Schematic diagram of the experimental setup. (2) Simulations of the radial motion of 5- and 10-μm air bubbles at atmospheric pressure in *n*-hexane. (3) Simulations of the radial motion of 5- and 10-μm air bubbles at elevated (2.5 bar) pressure in *n*-hexane. (4) An Excel file listing all the kinetic data for the reactions, along with fitted data with first-order kinetic model and the regression constants. This material is available free of charge via the Internet at http://pubs.acs.org.

■ AUTHOR INFORMATION

Corresponding Author

*Fax: +91 361 258 2291. E-mail: vmoholkar@iitg.ernet.in.

Notes

The authors declare no competing financial interest.

■ ACKNOWLEDGMENTS

H.A.C. acknowledges the Ministry of New and Renewable Energy, Govt. of India, for financial assistance through a National Renewable Energy Fellowship. The authors are also grateful to the anonymous referees of this paper for their meticulous evaluation and constructive criticism.

■ REFERENCES

(1) Mei, H.; Mei, B. W.; Yen, T. F. A New Method for Obtaining Ultra-Low Sulphur Diesel Fuel via Ultrasound Assisted Oxidative Desulphurization. *Fuel* **2003**, *82*, 405.

(2) Deshpande, A.; Bassi, A.; Prakash, A. Ultrasound Assisted, Base Catalyzed Oxidation of 4,6-Dimethyl Dibenzothiophene in Biphasic Diesel−Acetonitrile System. *Energy Fuels* **2005**, *19*, 28.

(3) Wan, M.-W.; Yen, T.-F. Enhance Efficiency of Tetraoctyl Ammonium Fluoride Applied to Ultrasound Assisted Oxidative Desulphurization (UAOD) Process. *Appl. Catal., A* **2007**, *319*, 237.

(4) Dai, Y.; Qi, Y.; Zhao, D.; Zhang, H. An Oxidative Desulphurization Method Using Ultrasound/Fenton's Reagent for Obtaining Low and/or Ultra-low Sulfur Diesel Fuel. *Fuel Process. Technol.* **2008**, *89*, 927.

(5) Mello, P.; de, A.; Duarte, F. A.; Nunes, M. A. G.; Alencar, M. S.; Moreira, E. M.; Korn, M.; Dressler, V. L.; Flores, E. M. M. Ultrasound Assisted Oxidative Process for Sulfur Removal from Petroleum Product Feedstock. *Ultrason. Sonochem.* **2009**, *16*, 732.

(6) Wu, Z.; Ondruschka, B. Ultrasound-Assisted Oxidative Desulphurization of Liquid Fuels and Its Industrial Application. *Ultrason. Sonochem.* **2010**, *17*, 1027.

(7) Kuppa, R.; Moholkar, V. S. Physical features of ultrasound-enhanced heterogeneous permanganate oxidation. *Ultrason. Sonochem.* **2010**, *17* (1), 123.

(8) Sivasankar, T.; Paunikar, A. W.; Moholkar, V. S. Mechanistic Approach to Enhancement of the Yield of a Sonochemical Reaction. *AIChE J.* **2007**, *53*, 1132.

(9) Krishnan, S. J.; Dwivedi, P.; Moholkar, V. S. Numerical Investigation into the Chemistry Induced by Hydrodynamic Cavitation. *Ind. Eng. Chem. Res.* **2006**, *45*, 1493.

(10) Toegel, R.; Gompf, B.; Pecha, R.; Lohse, D. Does water vapor prevent upscaling sonoluminescence? *Phys. Rev. Lett.* **2000**, *85*, 3165.

(11) Storey, B. D.; Szeri, A. J. Water Vapor, Sonoluminescence and Sonochemistry. *Proc. R. Soc. London, Ser. A* **2000**, *456*, 1685.

(12) Reid, R. C.; Prausnitz, J. M.; Poling, B. E. *Properties of Gases and Liquids*; McGraw−Hill: New York, 1987.

(13) Hirschfelder, J. O.; Curtiss, C. F.; Bird, R. B. *Molecular Theory of Gases and Liquids*; Wiley: New York, 1954.

(14) Condon, E. U.; Odishaw, H. *Handbook of Physics*; McGraw−Hill: New York, 1958.

(15) Zhou, J.; Lu, X.; Wang, Y.; Shi, J. Molecular Dynamics Investigation on the Finite Dilute Diffusion Coefficients of Organic Compounds in Supercritical Carbon Dioxide. *Fluid Phase Equilib.* **2000**, *172*, 279.

(16) Zhu, Y.; Lu, X.; Zhou, J.; Wang, Y.; Shi, J. Prediction of Diffusion Coefficients for Gas, Liquid and Supercritical Fluid: Application to Pure Real Fluids and Infinite Dilute Binary Solutions Based on the Simulations of Lennards-Jones Fluid. *Fluid Phase Equilib.* **2000**, *194−197*, 1141.

(17) Press, W. H.; Teukolsky, S. A.; Flannery, B. P.; Vetterling, W. T. *Numerical Recipes*; Cambridge University Press: New York, 1992.

(18) Eriksson, G. Thermodynamic studies of high temperature equilibria—XII: SOLGAMIX, a computer program for calculation of equilibrium composition in multiphase systems. *Chem. Scr.* **1975**, *8*, 100.

(19) Sivasankar, T.; Moholkar, V. S. Mechanistic Approach to Intensification of Sonochemical Degradation of Phenol. *Chem. Eng. J.* **2009**, *149*, 57.

(20) Pierce, A. D. *Acoustics: An Introduction to Its Physical Principles and Application*; Acoustical Society of America: New York, 1989.

(21) Reid, R. C.; Prausnitz, J. M.; Poling, B. E. *Properties of Gases and Liquids*; McGraw Hill: New York, 1987.

(22) Hirschfelder, J. O.; Curtiss, C. F.; Bird, R. B. Molecular Theory of Gases and Liquids; Wiley: New York, 1954.

(23) Condon, E. U.; Odishaw, H. *Handbook of Physics*; McGraw Hill: New York, 1958.

(24) Zhou, J.; Lu, X.; Wang, Y.; Shi, J. Molecular Dynamics Investigation on the Finite Dilute Diffusion Coefficients of Organic Compounds in Supercritical Carbon Dioxide. *Fluid Phase Equilib.* **2000**, *172*, 279.

(25) Zhu, Y.; Lu, X.; Zhou, J.; Wang, Y.; Shi, J. Prediction of Diffusion Coefficients for Gas, Liquid and Supercritical Fluid: Application to Pure Real Fluids and Infinite Dilute Binary Solutions Based on the Simulations of Lennards−Jones Fluid. *Fluid Phase Equilib.* **2000**, *194−197*, 1141.